AD-A186 022 HIGH RESOLUTION SIMULATION OF TURBULENT FLOW IN A CHANNEL(U) NAVAL RESEARCH LAB WASHINGTON DC R A HANDLER ET AL 25 SEP 87 NRL-MR-6009 1/1

UNCLASSIFIED F/G 20/4 NL

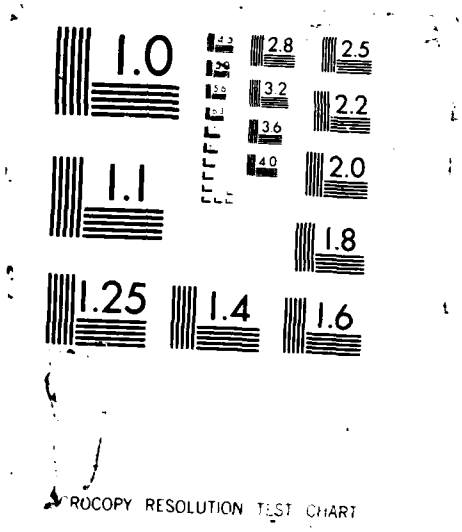
1.0
2.8
2.5
3.2
2.2
3.6
4.0
2.0
1.1
1.8
1.25
1.4
1.6
ROCOPY RESOLUTION TEST CHART

Naval Research Laboratory
Washington, DC 20375-5000

NRL Memorandum Report 6009

High Resolution Simulation of Turbulent Flow in a Channel

R.A. HANDLER, R.I. LEIGHTON AND D.M. CARROLL

Center for Fluid/Structure Interactions
Laboratory for Computational Physics and Fluid Dynamics

September 25, 1987

SECURITY CLASSIFICATION OF THIS PAGE

REPORT DOCUMENTATION PAGE

1a. REPORT SECURITY CLASSIFICATION UNCLASSIFIED	1b. RESTRICTIVE MARKINGS
2a. SECURITY CLASSIFICATION AUTHORITY	3. DISTRIBUTION/AVAILABILITY OF REPORT Approved for public release; distribution unlimited.
2b. DECLASSIFICATION/DOWNGRADING SCHEDULE	
4. PERFORMING ORGANIZATION REPORT NUMBER(S) NRL Memorandum Report 6009	5. MONITORING ORGANIZATION REPORT NUMBER(S)
6a. NAME OF PERFORMING ORGANIZATION Naval Research Laboratory 6b. OFFICE SYMBOL (If applicable) Code 4420	7a. NAME OF MONITORING ORGANIZATION Office of Naval Research
6c. ADDRESS (City, State, and ZIP Code) Washington, DC 20375-5000	7b. ADDRESS (City, State, and ZIP Code) Arlington, VA 22217
8a. NAME OF FUNDING/SPONSORING ORGANIZATION Office of Naval Research 8b. OFFICE SYMBOL (If applicable)	9. PROCUREMENT INSTRUMENT IDENTIFICATION NUMBER
8c. ADDRESS (City, State, and ZIP Code) Arlington, VA 22217	10. SOURCE OF FUNDING NUMBERS PROGRAM ELEMENT NO. 61153N; PROJECT NO.; TASK NO. RR023-01-41; WORK UNIT ACCESSION NO. DN880-019
11. TITLE (Include Security Classification) High Resolution Simulation of Turbulent Flow in a Channel	
12. PERSONAL AUTHOR(S) Handler, R.A., Leighton, R.I. and Carroll, D.M.	
13a. TYPE OF REPORT Interim 13b. TIME COVERED FROM 3/86 TO 3/87	14. DATE OF REPORT (Year, Month, Day) 1987 September 25 15. PAGE COUNT 31
16. SUPPLEMENTARY NOTATION	
17. COSATI CODES FIELD / GROUP / SUB-GROUP	18. SUBJECT TERMS (Continue on reverse if necessary and identify by block number) Turbulence, Simulation Conditional sampling

19. ABSTRACT (Continue on reverse if necessary and identify by block number)

A simulation of turbulence in a channel is performed using 128 × 64 × 65 grid points. No turbulence models are incorporated in the calculation. After an initial lower resolution run, the flow is driven by a constant force. At the end of the run, which lasts 54.4 time units, the flow achieves a dynamic equilibrium in the sense that the wall shear stress is balanced almost exactly by the driving force. The global properties of the flow are discussed in detail and some initial results of coherent structures using conditional sampling are presented.

20. DISTRIBUTION/AVAILABILITY OF ABSTRACT ☒ UNCLASSIFIED/UNLIMITED ☐ SAME AS RPT. ☐ DTIC USERS	21. ABSTRACT SECURITY CLASSIFICATION UNCLASSIFIED
22a. NAME OF RESPONSIBLE INDIVIDUAL Robert A. Handler	22b. TELEPHONE (Include Area Code) (202) 767-2457 22c. OFFICE SYMBOL Code 4420

DD FORM 1473, 84 MAR 83 APR edition may be used until exhausted. All other editions are obsolete.

SECURITY CLASSIFICATION OF THIS PAGE

CONTENTS

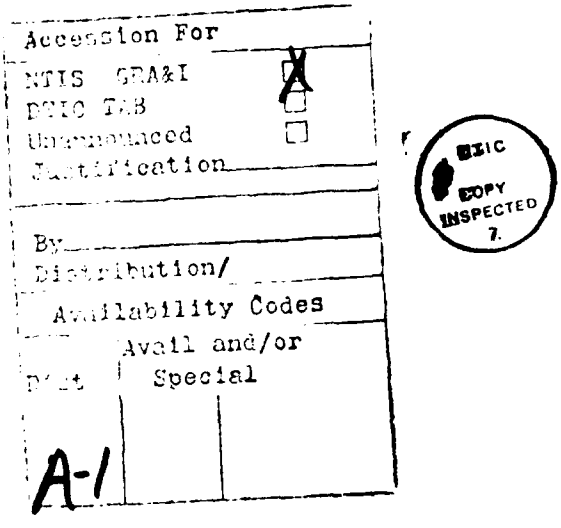

HIGH RESOLUTION SIMULATION OF TURBULENT FLOW IN A CHANNEL

INTRODUCTION

The primary purpose of the current work is to perform a high resolution, statistically stationary simulation of turbulent flow in a channel. High resolution is of critical importance as the following review of the experimental facts will show. It is well known, for example, that the turbulent structures near the wall are highly elongated with a streamwise wave length several times greater than the spanwise wavelength. The characteristic spanwise wavelength is known to be on the order of 100 viscous lengths. The viscous length, l^*, is defined by ν/u^*, where ν is the kinematic viscosity and u^* is the friction velocity given by $\sqrt{\tau_w/\rho}$, where τ_w is the shear stress at the wall and ρ is the density. It has been shown by numerous experimental studies that this "streaky" structure is clearly associated with a process called bursting. It is this bursting process which is apparently responsible for the production of new turbulence in shear flows. For this reason, it is essential that the spanwise resolution of the calculation be as high as possible. In the present Cray-XMP calculation we used the highest possible resolution consistent with our code and with current machine memory limitations. The simulation represents turbulence in a channel using (128) $\times$ 64 $\times$ 65 grid points, where the spanwise (x_3) direction was represented by 128 points, the streamwise (x_1) direction by 64 points, and the wall-normal (x_2) direction by 65 points.* The channel size (based on channel half-width) is 2 in the wall-normal direction and 5 in both the streamwise and spanwise directions. This gives a spanwise resolution, $\Delta x_3/l^*$, of 6.6, which should be more than adequate to resolve the near-wall structures.

Manuscript approved April 8, 1987.

Achieving a statistically stationary state is also of considerable importance. In previous direct simulations of turbulent channel flow by Orszag & Patera,[1] the flow is driven by a constant driving force which is chosen to maintain the original Poiseuille flow. The introduction of highly unstable disturbances causes transition to turbulence so that the wall shear stress coefficient increases and a quasistationary state is achieved. However, the mean wall shear stress must eventually return to its original laminar value and the final state of the flow may or may not be laminar. This kind of simulation is unsatisfactory since it produces only a very short burst of quasi-stationary turbulence. To overcome this difficulty, the present simulation was carried out in two stages. First, a lower resolution calculation using $64 \times 64 \times 65$ grid points was started from laminar initial conditions with a driving force which was constantly adjusted to match the wall shear stress. This resulted in a reasonably stationary flow with a driving force of about $6.06/R$, where $R = \frac{1}{\nu}$. This initial calculation was terminated at about 75 time units, where time is made non-dimensional on the channel half width, h, and the laminar centerline velocity, U. Once this quasistationary state was achieved, the data was interpolated to achieve the higher spanwise resolution and the second stage of the calculation was initiated. At this point the driving force was set equal to $6.0/R$. This value is maintained throughout the rest of the calculation.

NUMERICAL METHODS

The numerical methods used here have been developed by Orszag and others. The simulation involves obtaining approximate solutions to the following problem:

$$\frac{\partial \vec{u}}{\partial t} = \vec{u} \times \vec{\omega} - \vec{\nabla} \Pi + \frac{1}{R} \nabla^2 \vec{u} + \vec{f}$$

$$\Pi = p + \frac{1}{2} |\vec{u}|^2 \tag{1}$$

$$\vec{\nabla} \cdot \vec{u} = 0$$

*(The notation x, y, and z will be used to denote streamwise, spanwise, and wall-normal coordinates when the use of subscripts 1, 3, and 2 is cumbersome.)

and

$$\vec{u} = 0 \text{ at } x_2 = \pm 1$$

where the channel walls are at $x_2 = \pm 1$. All variables in equation (1) are made non-dimensional with h, U and ρ. We also define $\vec{u}$, the velocity, $\vec{\omega}$, the vorticity, p, the pressure, and $\vec{f}$, an externally applied force field.

The problem is solved by a pseudospectral or collocation method in which the velocity is expressed by:

$$\vec{u}(x,y,z,t) = \sum_{m=-M/2}^{M/2-1} \sum_{n=-N/2}^{N/2-1} \sum_{j=0}^{J} \vec{a}_{mnj}(t) e^{2\pi i \left(\frac{mx}{X} + \frac{ny}{Y} \right)} T_j(z) \tag{2}$$

Here, X and Y represent, respectively, the streamwise and spanwise lengths of the domain. The problem is discretized by choosing the collocation points as follows:

$$x_i = i \frac{X}{M} \qquad i = 0 \ldots M - 1$$

$$y_j = j \frac{Y}{N} \qquad j = 0 \ldots N - 1$$

$$z_k = \cos \frac{\pi k}{J} \qquad k = 0 \ldots J .$$

The Fourier coefficients, $\vec{a}_{mnj}$, are computed efficiently using one dimensional fast Fourier transforms. Derivatives then can be calculated in Fourier space and transformed back to real space without introducing phase errors.

The time stepping is split into three intermediate problems. In the first step, the non-linear term, $(\vec{u} \times \vec{\omega})$, is computed directly in real space and used to correct the current velocity field using an Adams-Bashforth explicit time stepping scheme of second order. The incompressibility condition is then imposed by inverting the Poisson equation for the pressure and satisfying the inviscid boundary condition that the normal velocity on both walls is zero. In the final step, the viscous correction

is added together with the no-slip boundary condition at the walls. Further details on the numerical scheme can be found in Orszag & Kells.[2]

RESULTS

A. Global Properties

The global properties of the flow are shown in Figures 1 and 2. In Figure 1 the Reynolds number, R^*, ($R^* = u_* h / \nu$) is plotted against computational time. The entire computational run time (0 - 54.4) is shown. It is important to note that in a physical experiment, the flow is driven by a pressure gradient. In the simulation, however, periodic boundary conditions are used in the horizontal plane so that a differential pressure forcing cannot be prescribed. This requires the use of the external driving force, $\bar{f}$, in the equation of motion. We note, of course, that $\bar{f}$ is a completely arbitrary function of space and time. If we define a control surface to be that which encloses the entire computational domain, a simple momentum balance in the streamwise direction results in:

$$\frac{\partial}{\partial t} \int_1^1 <u_1> dz = \frac{-2<\tau_0>}{\rho U^2} + \frac{2<f_1> h}{\rho U^2} \tag{3}$$

In this expression, $< >$ represents averaging in the horizontal plane, τ_0 is the instantaneous shear stress at the wall, and f_1 is the streamwise force per unit volume. The simple form of this expression is due to the use of periodic boundary conditions which insure no net mass flow through the control surface and no net force arising from normal stresses (pressure). It follows from this that for a globally steady flow the time rate of change in momentum within the control volume must be zero so that $\lim_{t \to \infty} <\tau_0> = h \lim_{t \to \infty} <f_1>$. This can be written more conveniently as:

$$\lim_{t \to \infty} R^*(t) = \lim_{t \to \infty} \sqrt{\frac{<f_1> h}{\rho U^2} R^2} \tag{4}$$

In this calculation, the driving force is set to $6/R$ so that the flow is forced to achieve a steady

state value of $R^* = \sqrt{6R}$ which is 173.2 for $R = 5000$ (a value which was fixed throughout the calculation). We can see readily from Figure 1 that at the end of calculation R^* is within about 0.5% of the theoretical value and is never more than 5% lower than theory throughout the entire calculation. Thus, for all practical purposes, the turbulence has achieved a dynamic equilibrium. It is also important to note that this state cannot decay to a laminar or quasi-laminar state as in the calculation of Orszag because of the maintenance of a high streamwise driving force. There is no reason to believe that the turbulence cannot be maintained indefinitely. We should also note, however, that scaling arguments show that the flow evolves over a viscous time period of order R so that for true stationarity we must calculate for about 5000 time units. This is clearly well beyond the currently available resources so that we must be content with something that is not completely stationary.

In Figure 2 we plot the average streamwise velocity at the center of the channel, U_{cl}, against computational time. The centerline velocity has been made nondimensional with the initial laminar centerline velocity, U. It appears to be slowly decreasing during the course of the run. This result is not, however, inconsistent with the fact that the imposed driving force is always larger than the wall shear stress since the force balance (Eq. 3) shows that the mass flux (not necessarily U_{cl}) must be increasing with time. It is also interesting to note that the R^* time record of Figure 1 shows high frequency fluctuations which are not present in the centerline velocity data of Figure 2. This is most likely a real effect due to the much shorter time scales near the wall.

We also examine the stationarity of the flow by observing changes in the mean streamwise velocity profile and the root mean square amplitude of the turbulence intensities as the calculation proceeds. In each of the succeeding figures, we plot results at times of 0, 12.825, 25.65, 38.48, and 51.3. In Figure 3 we plot the mean streamwise velocity scaled on u_* against wall normal distance x_2^*, defined as x_2/l^*. At $t = 51.3$, three regions of the profile are clearly identified: (a) the viscous sublayer ($x_2^* \leq 2$), (b) a buffer layer ($2 \leq x_2^* \leq 30$) and, (c) a logarithmic layer

($30 \leq x_2^* \leq 120$). There is also a core region extending out to $x_2^* = 173$. The significance of this is that very early in the calculation the logarithmic layer was not at all evident. The logarithmic region at $t = 51.3$ can be approximated by the so-called law of the wall, $<u_1> / u^* = k \ln x_2^* + c$, where $k = 3.28$ and $c = 6.32$. Most experimental results for channel flow give k between 2.5 and 3 and c varies from 4 to 6. The calculated values are somewhat higher for both constants.

In Figures 4-7, we plot the rms magnitudes of u_1, u_2, u_3, and u_1u_2 against x_2^*. The most interesting feature in Figure 4 is the distinct shift in the x_2^* location of the maximum of $<u_1^2> / u^*$ towards the wall as the calculation proceeds. The location of the peak shifts from about 40 at the start of the run to about 23 at the end. This is an encouraging trend since it is known from the experiments of Kreplin and Eckelmann[3] at about the same Reynolds number that the peak occurs at about 13. Though the calculated location of the peak is still far from experiment, the trend suggests that more run time may bring the peak even closer to the wall. The calculated amplitude of $\sqrt{<u_1^2>} / u^*$ is somewhat lower than the value of 2.85 found in (3). In the Appendix (Figures A1 and A2) we show both the mean streamwise velocity and streamwise turbulence intensity profiles in greater detail. The peak value of $\sqrt{<u_2^2>} / u^*$ is about 0.96 at the end of the calculation and occurs at about $x_2^* \simeq 100$, as shown in Figure 5. This is very close to the value of 1.0 obtained experimentally by Clark[4] at $x_2^* = 70$. The $\sqrt{<u_3^2>} / u^*$ profile peaks at about 1.31 at the end of calculation and occurs at $x_2^* \simeq 50$ as shown in Figure 6. Clark measured a peak of about 1.25 at $x_2^* \simeq 25$. The $<u_1u_2> / u^{*2}$ profile peaks at about 0.64 at the end of the calculation and occurs at $x_2^* \simeq 50$.

As an aid in examining, at least qualitatively, the structure of the turbulence, we plot in Figure 8 (a-d), contours of u_1, in horizontal planes at several distances from the wall. On each figure we plot two contour levels, $(u_1 - <u_1>) - u_1'$ and $(u_1 - <u_1>) - 1/4\, u_1'$ where u_1' is the rms

magnitude. We have chosen to plot these contour levels since they correspond to the low speed regions of the flow normally observed in experimental flow visualization studies.

In the sublayer ($x_2^* = 1.86$) we note that the structure is distinctly elongated in the streamwise direction. In the buffer layer, ($x_2^* = 10.1$), a similar structure is apparent but the average size of the structures has grown. It cannot be determined definitely from these plots if a distinct spanwise wavelength corresponding to the well known streaky turbulent structure actually exists. This needs to be determined by more detailed spectral analysis in the future. However, if one can imagine a characteristic wavelength it is certainly not far from the accepted value of about 100, as mentioned earlier. At the bottom edge of the logarithmic layer ($x_2^* = 44.8$) the structures have grown noticeably larger, and well within the logarithmic layer ($x_2^* = 99.0$) the structures have grown to the size of the flow domain.

B. Conditional Sampling Results

In addition to the global results, the data generated by the numerical simulation has been examined by conditional sampling techniques. The object of conditional sampling is to detect regions in the flow which are of interest. The second quadrant Reynolds stress, where the fluctuating streamwise velocity is negative and the normal velocity is positive is, of considerable interest since it represents an ejection of fluid from the wall region. Also of interest are shear layers which exist close to the wall. These are detected by the Variable Interval Time Averaging (VITA) technique. These two conditional sampling techniques detect turbulent bursts, which are believed to be the major dynamical event responsible for the creation of turbulent kinetic energy and momentum transport from the wall.

Two sets of conditional sampling experiments have been performed using the data set described in the report. The first set of experiments is a direct continuation of the work started in Leighton[5].

Using the second quadrant Reynolds stress conditional sampling scheme, turbulent structures were detected in the simulated turbulent channel flow. The detections were performed at 10.2 and 16.8 viscous lengths from the wall, and the events were averaged in the x-z plane.

Figure 9 shows some typical results of the second quadrant Reynolds stress conditional sampling. The first contour plot is the streamwise fluctuating coherent velocity at the detection time. The second plot is the fluctuating normal velocity. Due to the choice of the coordinate system in the computations, fluid flowing away from the upper wall has a negative value. In the final figure, the second quadrant Reynolds stress is presented and is also positive due to the coordinate system.

Several conclusions can be drawn from these averages:

(1) They are consistent with the results obtained from the numerical simulation generated on a Cray 1 at Los Alamos National Laboratory, and described in (5).

(2) They show the event developing two structures. The region of second quadrant Reynolds stress, representing fluid that is being ejected from the wall, is initially farther away from the wall than the detection site. As the time approaches the detection time, the region of second quadrant Reynolds stress moves toward the wall. After detection the region continues to move toward the wall. A second region of second quadrant Reynolds stress appears slightly downstream and above the old region. This later region has not been detected in earlier work.

(3) The events detected closer to the wall are detected two to four viscous time units later than events farther from the wall, indicating that the region ejecting the fluid is moving toward the wall.

This work is continuing and a model of the turbulent ejection incorporating this information has not yet been developed.

SUMMARY AND CONCLUSIONS

A high resolution simulation of turbulence in a channel is performed using 128 × 64 × 65 grid points. The calculation achieves a resolution of $\Delta y/l^* = 6.6$ which should be sufficient to adequately resolve the organized structures near the wall. In addition, a dynamic equilibrium is achieved in which the shear forces at the wall are approximately balanced by a constant driving force. The flow, however, is not completely stationary as evidenced by a slowly dropping centerline velocity. At the end of the calculation, the mean velocity profile exhibits a well defined logarithmic layer.

In general, the magnitudes of peak root-mean-square values of the three components of the turbulent velocity fluctuations and the velocity correlation $<u_1u_2>$ agree well with experiment. The peaks occur somewhat farther from the wall than experimental measurements, but as the calculation proceeds, these locations appear to be moving closer to the wall. This behavior suggests that more computational time is needed to achieve true stationarity and results which are closer to experiment. Contour levels of the streamwise velocity at various locations above the wall show a clearly defined elongated structure near the wall. The structure becomes close to the scale of the horizontal domain in the logarithmic layer. In addition, conditional sampling of results indicate clearly defined coherent events.

ACKNOWLEDGEMENTS

This work was conducted as part of a research program in boundary layer hydrodynamics supported by the Naval Research Laboratory. Partial support for the computer time required to conduct the study was provided by the Office of Naval Research (Code 1132F).

REFERENCES

1. S.A. Orszag and A.T. Patera, "Calculation of Von Karman's Constant for Turbulent Channel Flow," Phys. Rev. Lett, Vol. 47, 832-835 (1981).

2. S.A. Orszag and L.C. Kells, "Transition to turbulence in plane Poiseuille and plane Couette Flow," J. Fluid Mech., Vol. 96, pp. 159-205.

3. Kreplin, H.-P. and Eckelmann, H., "Behavior of the Three Fluctucting Velocity Components in the Wall Region of a Turbulent Channel Flow," Phys. Fluids, Vol. 22, 1979, pp. 1233-1239.

4. J.A. Clark, "A Study of Incompressible Turbulent Boundary Layers in Channel Flow," ASME Transactions, J. Basic Engrg., Vol. 90, 1968, pp. 455-466.

5. R.I. Leighton, "Investigation of Burst Structures in a Turbulent Channel Flow Simulation using Conditional Sampling Techniques," Ph.D. Thesis, University of Michigan, 1986.

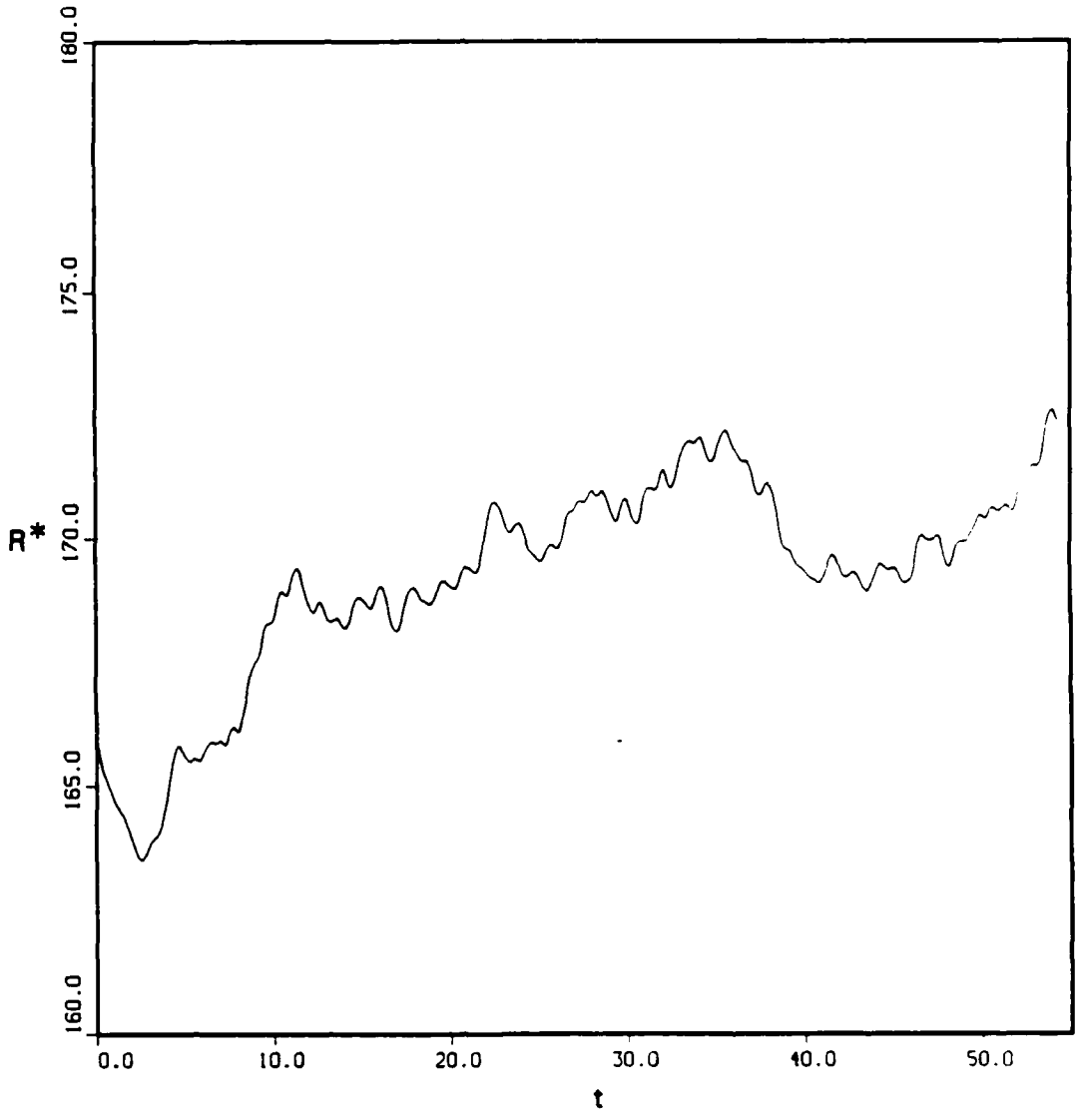

Fig. 1 — Reynolds number based on friction velocity versus computational time.

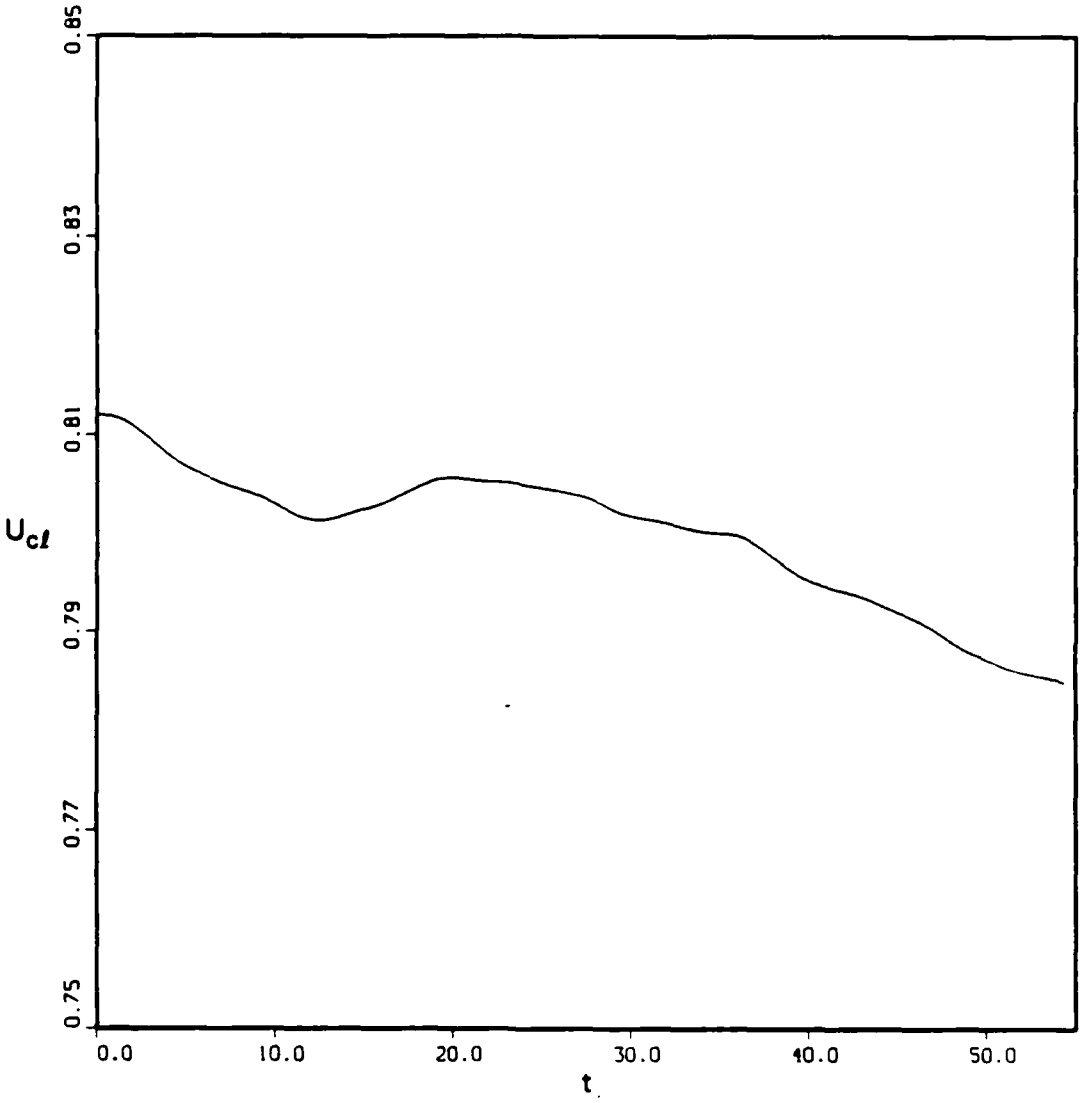

Fig. 2 — Centerline velocity versus computational time.

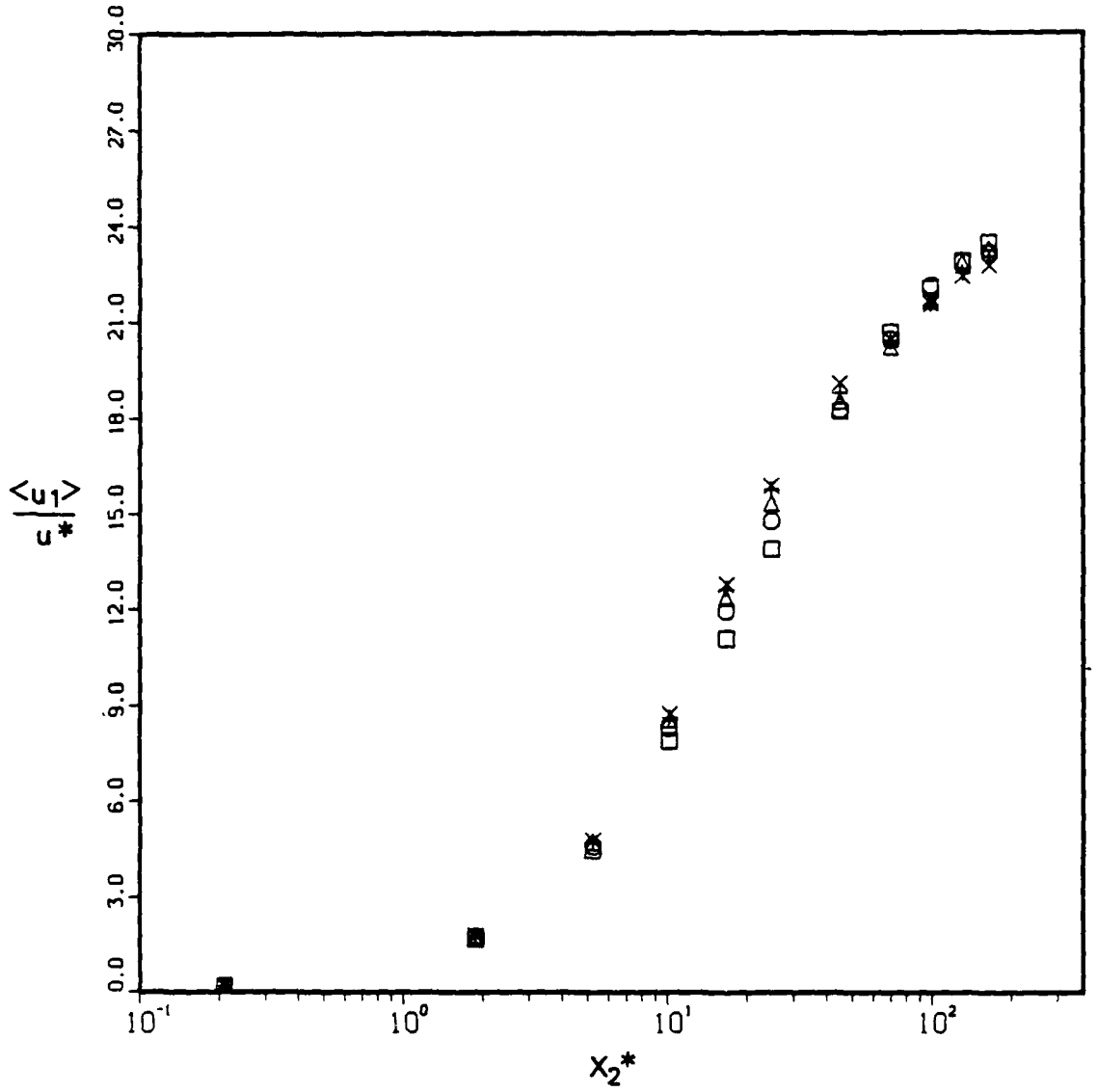

Fig. 3 — Mean streamwise velocity versus distance from the wall. □, $t = 0$; ○, $t = 12.825$; Δ, $t = 25.65$; +, $t = 38.48$; ×, $t = 51.3$. Note: These symbols apply to all succeeding figures.

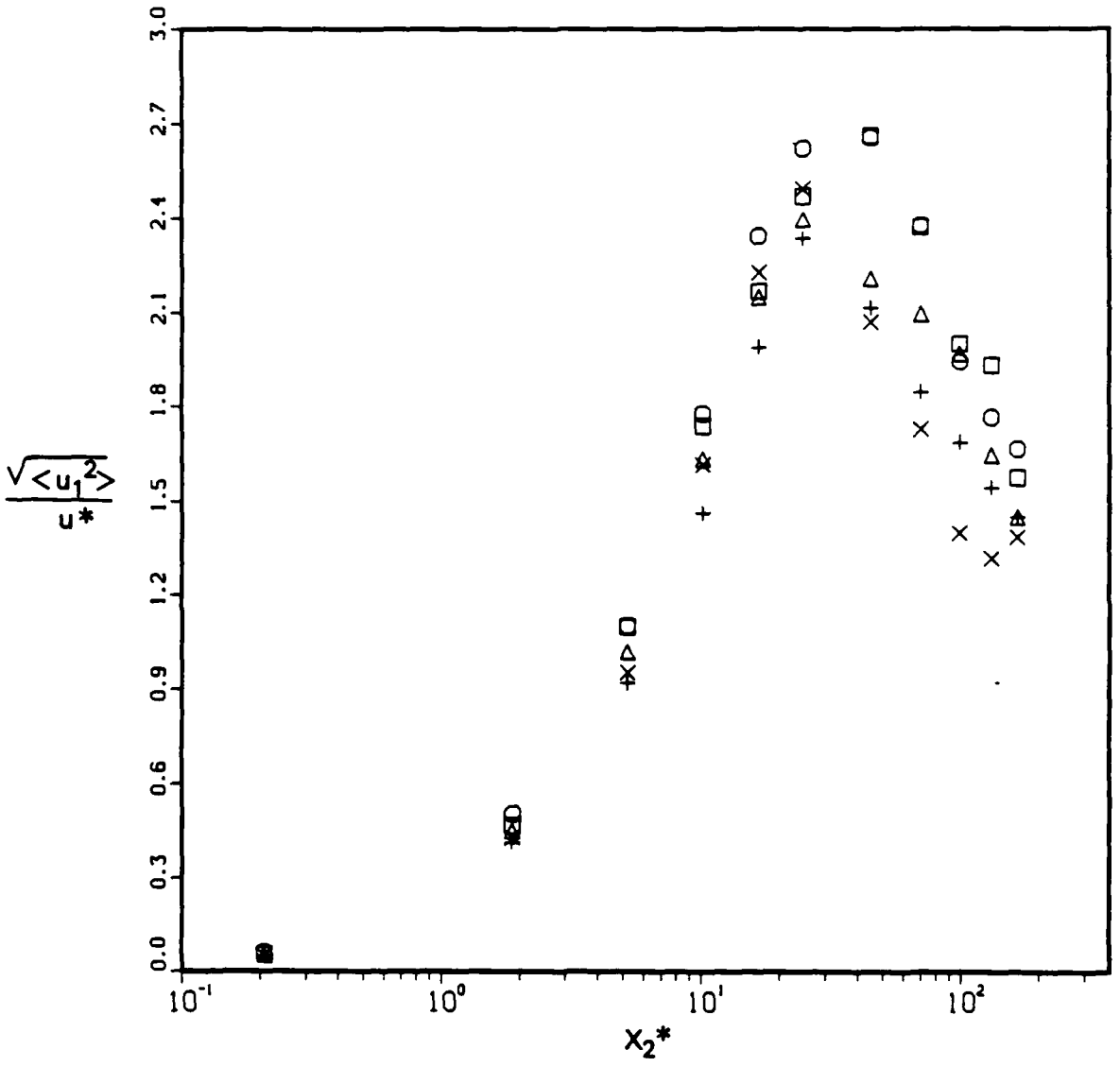

Fig. 4 — Root mean square streamwise velocity versus distance from the wall.

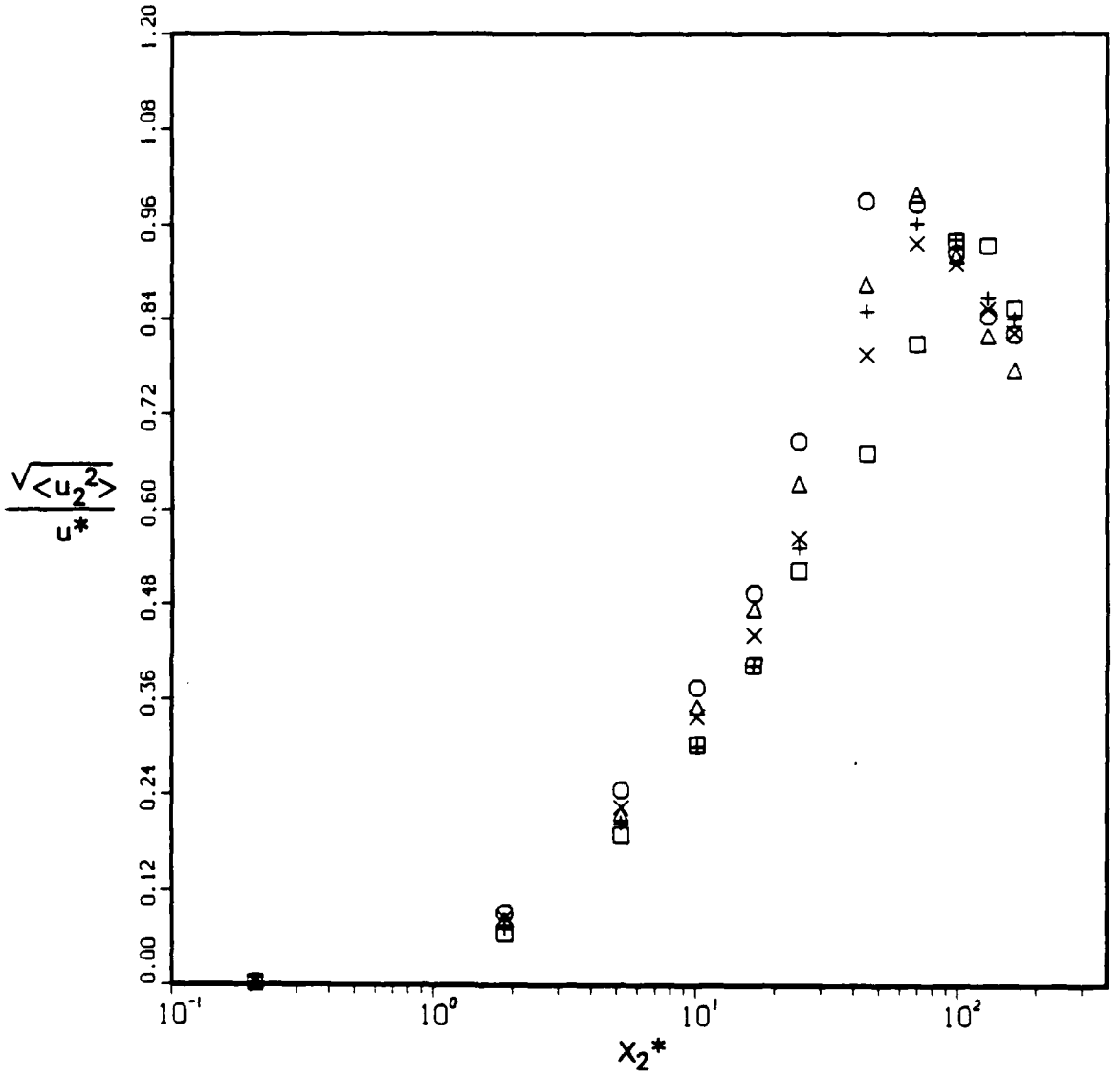

Fig. 5 — Root mean square wall-normal velocity versus distance from the wall.

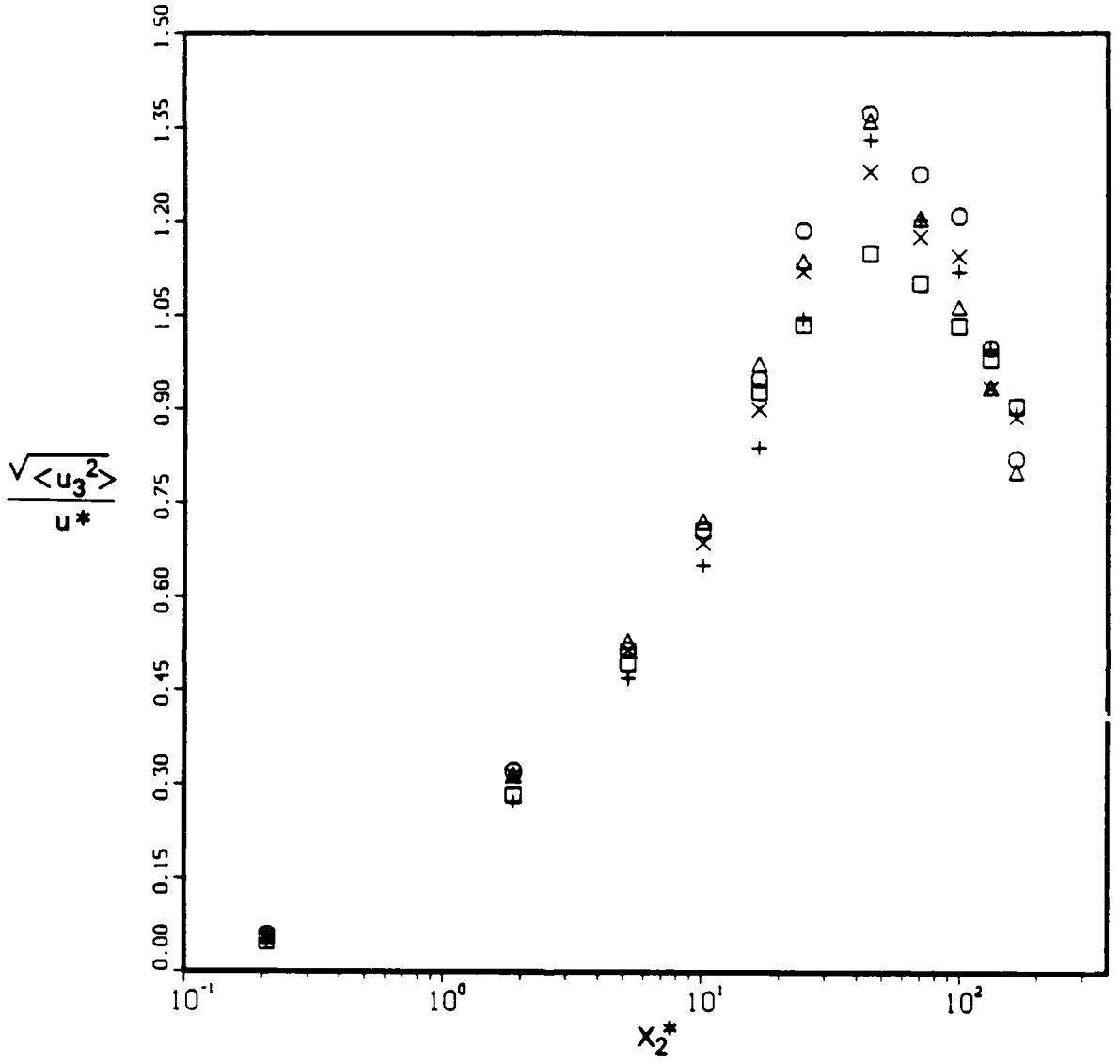

Fig. 6 — Root mean square spanwise velocity versus distance from the wall.

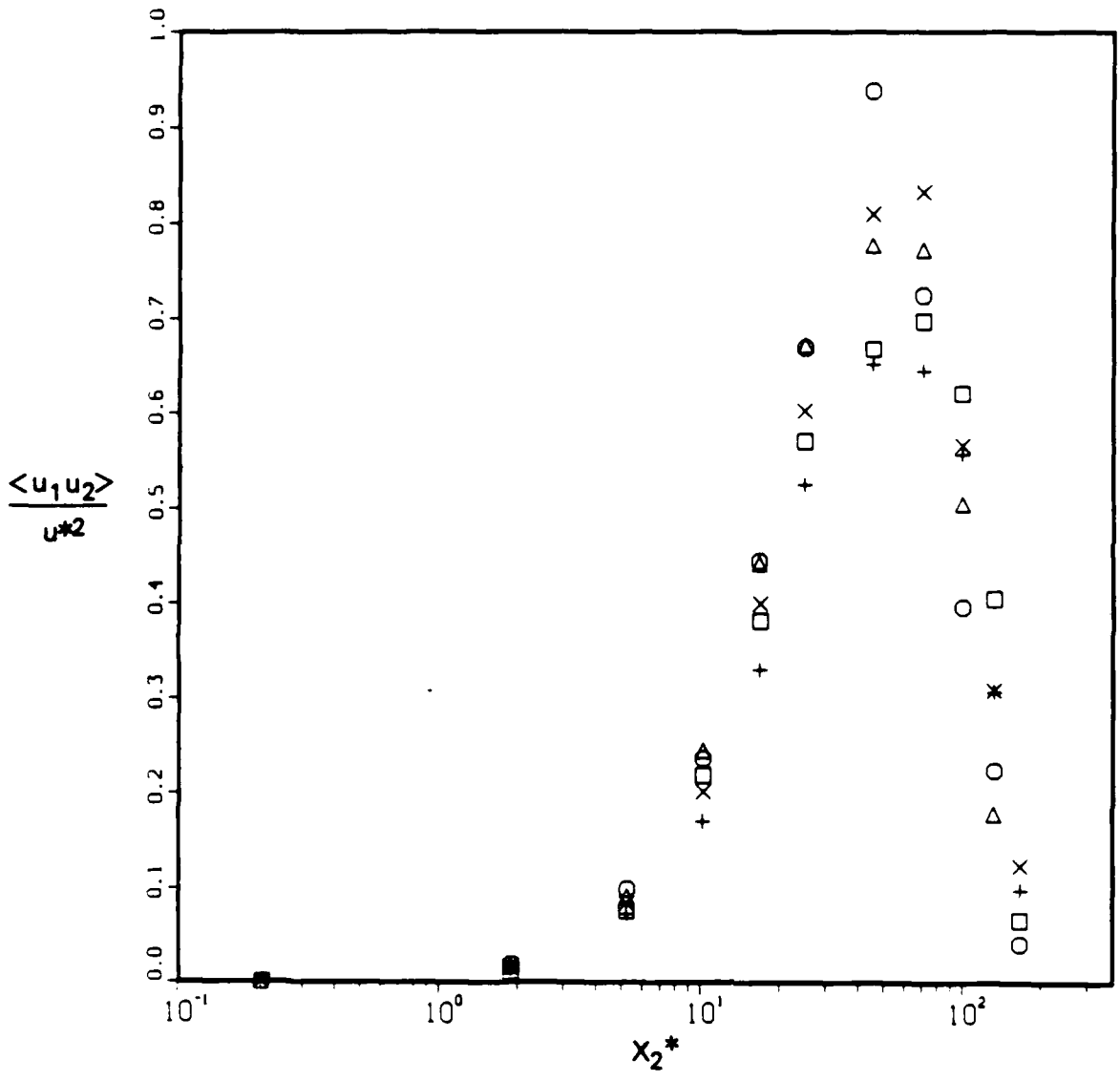

Fig. 7 — Reynolds stress versus distance from the wall.

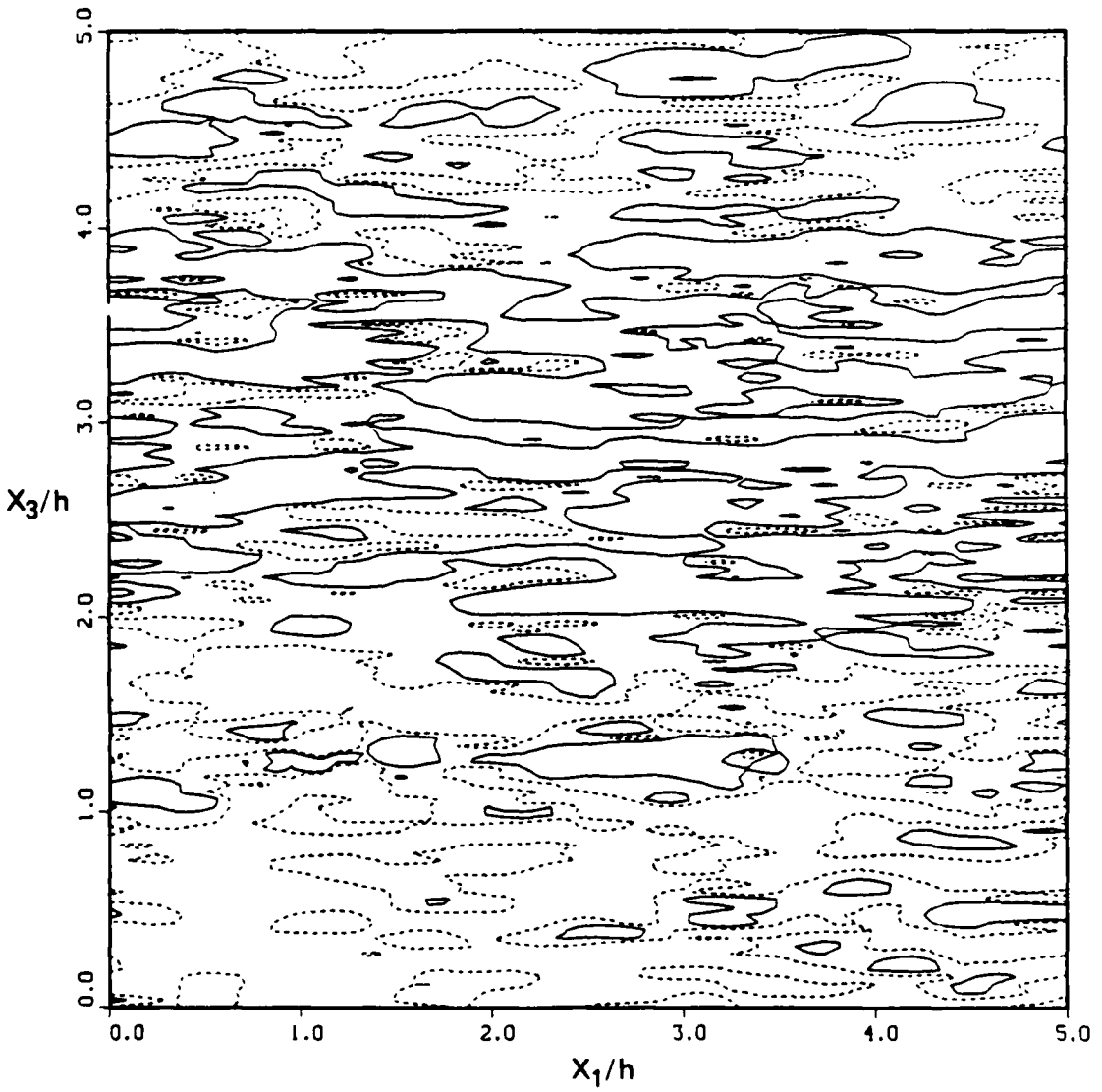

Fig. 8(a) — Contour plots of constant streamwise velocity at $x_2^* = 1.86$. Contour levels for figures 8 (a-d) are: Solid line $(u_1 - \langle u_1 \rangle) - (1/4)u_1'$,- - - - -,$(u_1 - \langle u_1 \rangle) - u_1'$.

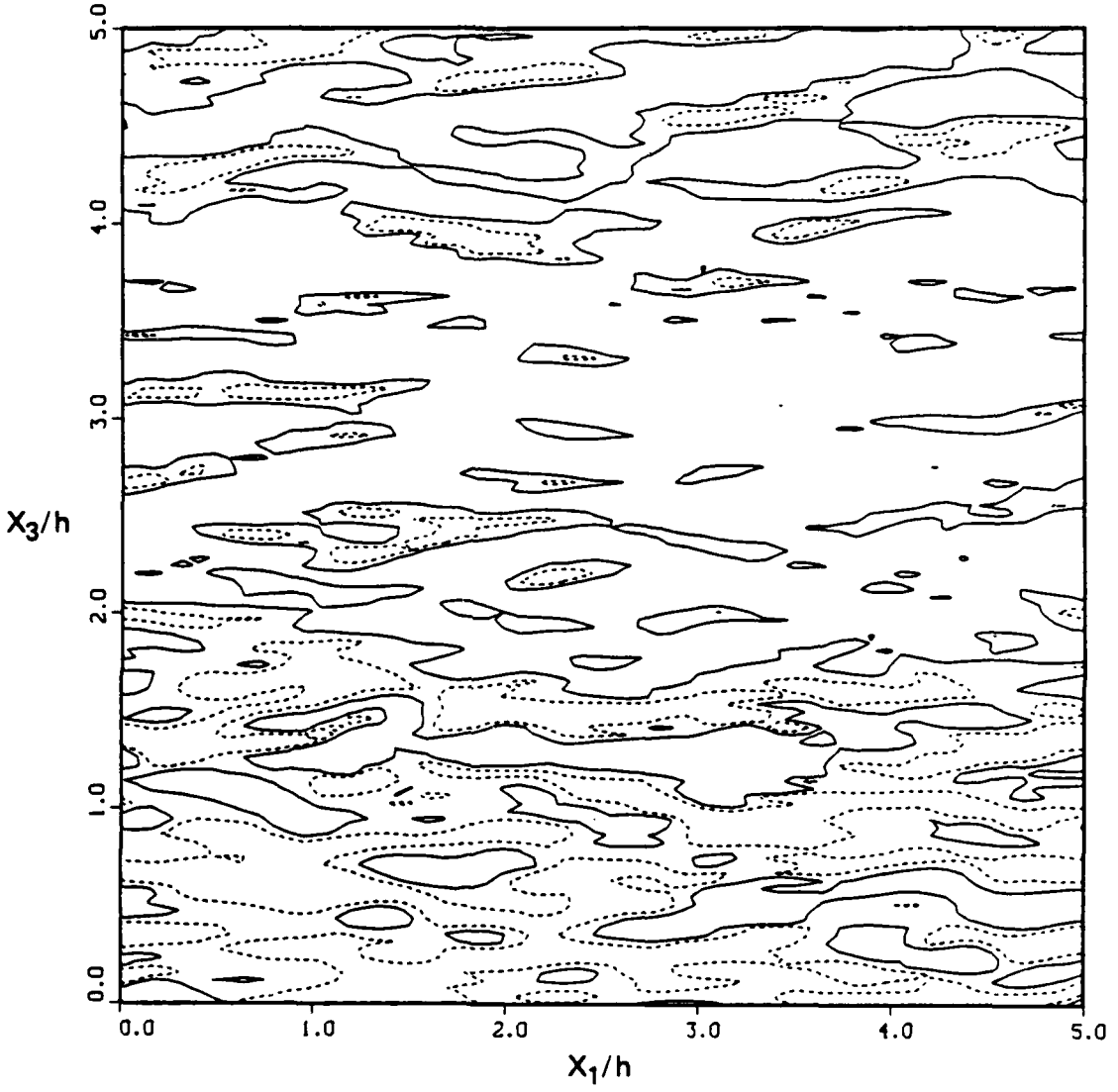

Fig 8(b) — Contour plots of constant streamwise velocity at $x_2^* = 10.1$.

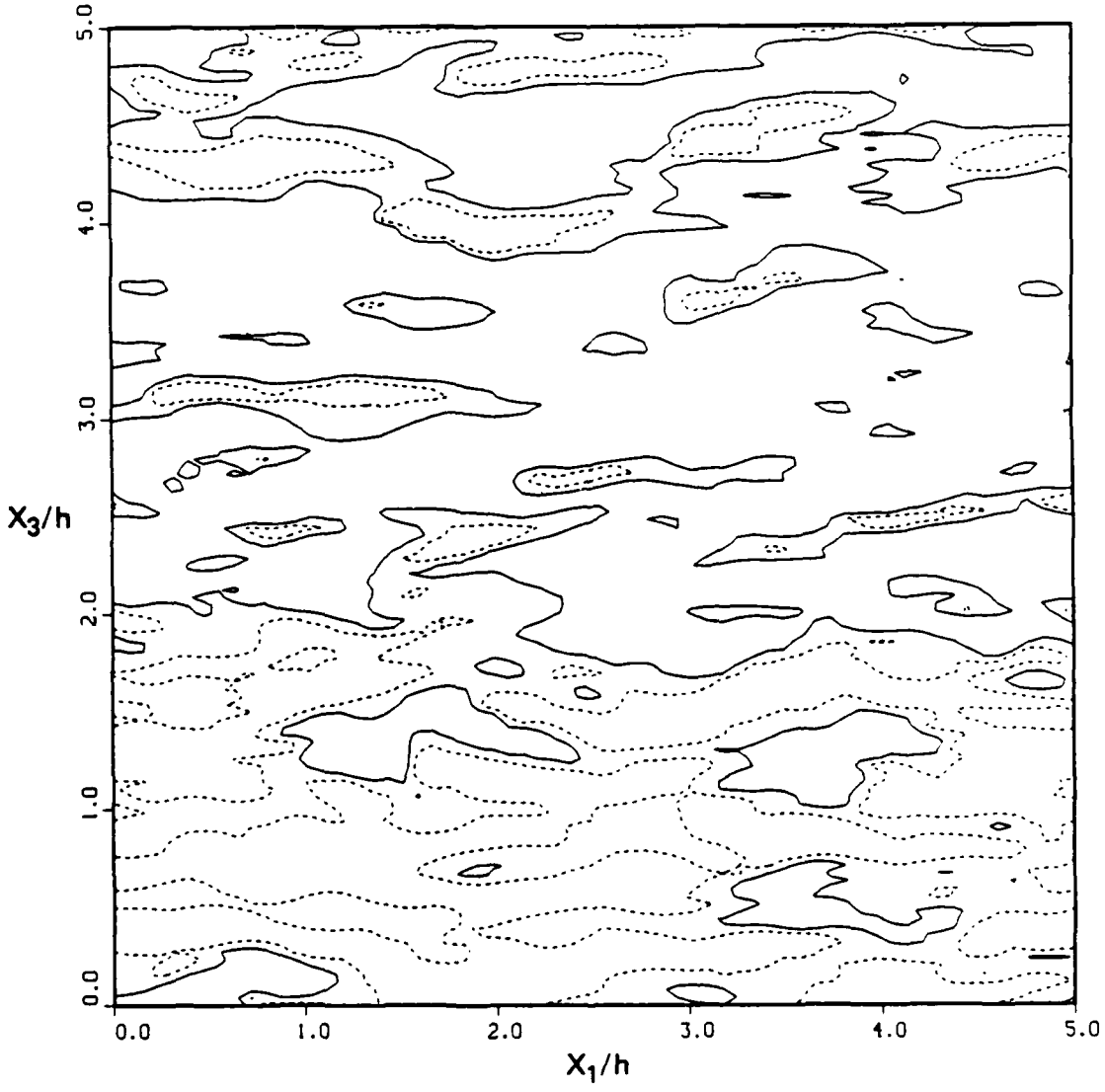

Fig. 8(c) — Contour plots of constant streamwise velocity at $x_2^* = 44.8$.

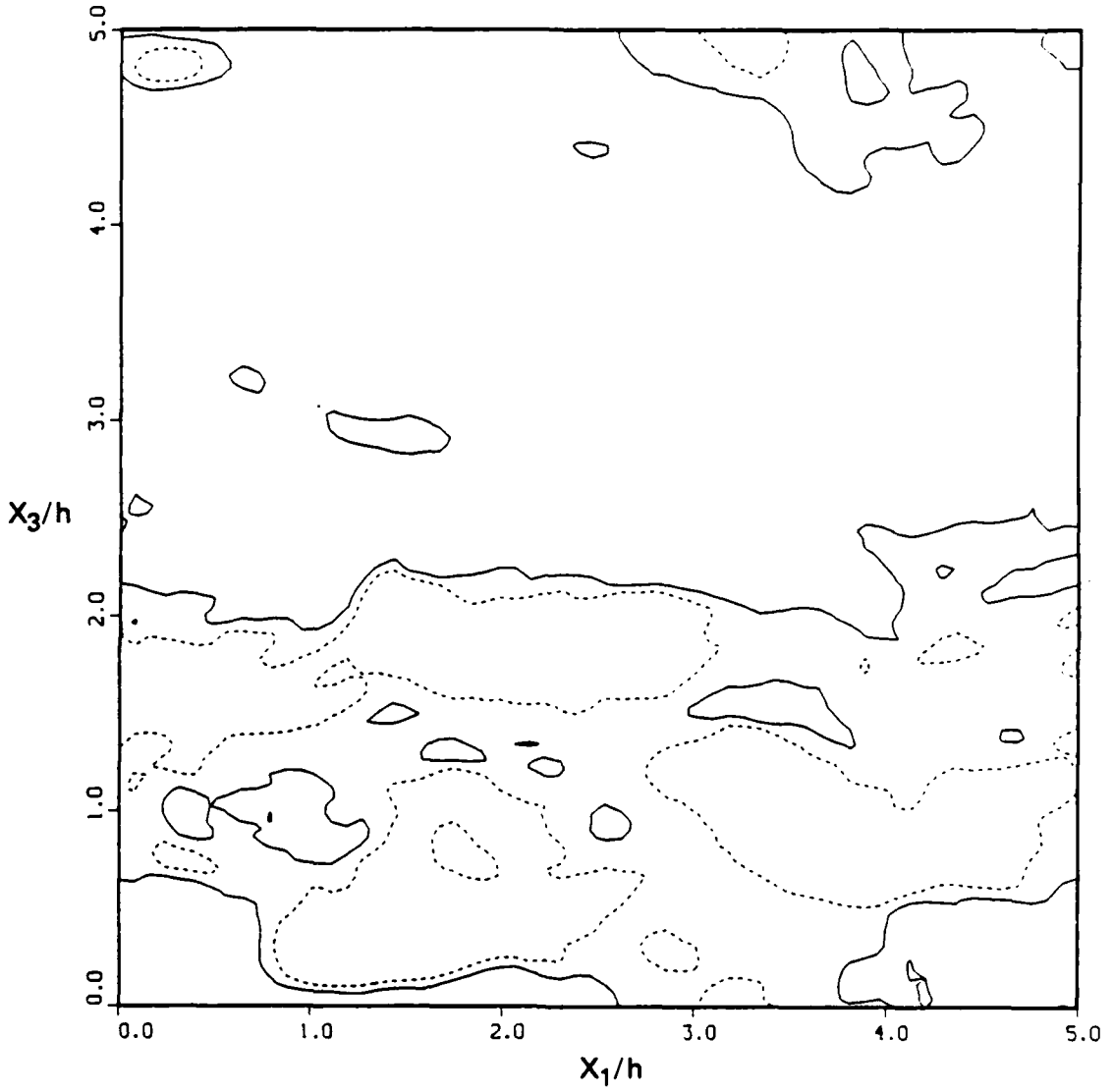

Fig. 8(d) — Contour plots of constant streamwise velocity at $x_2^* = 90.0$.

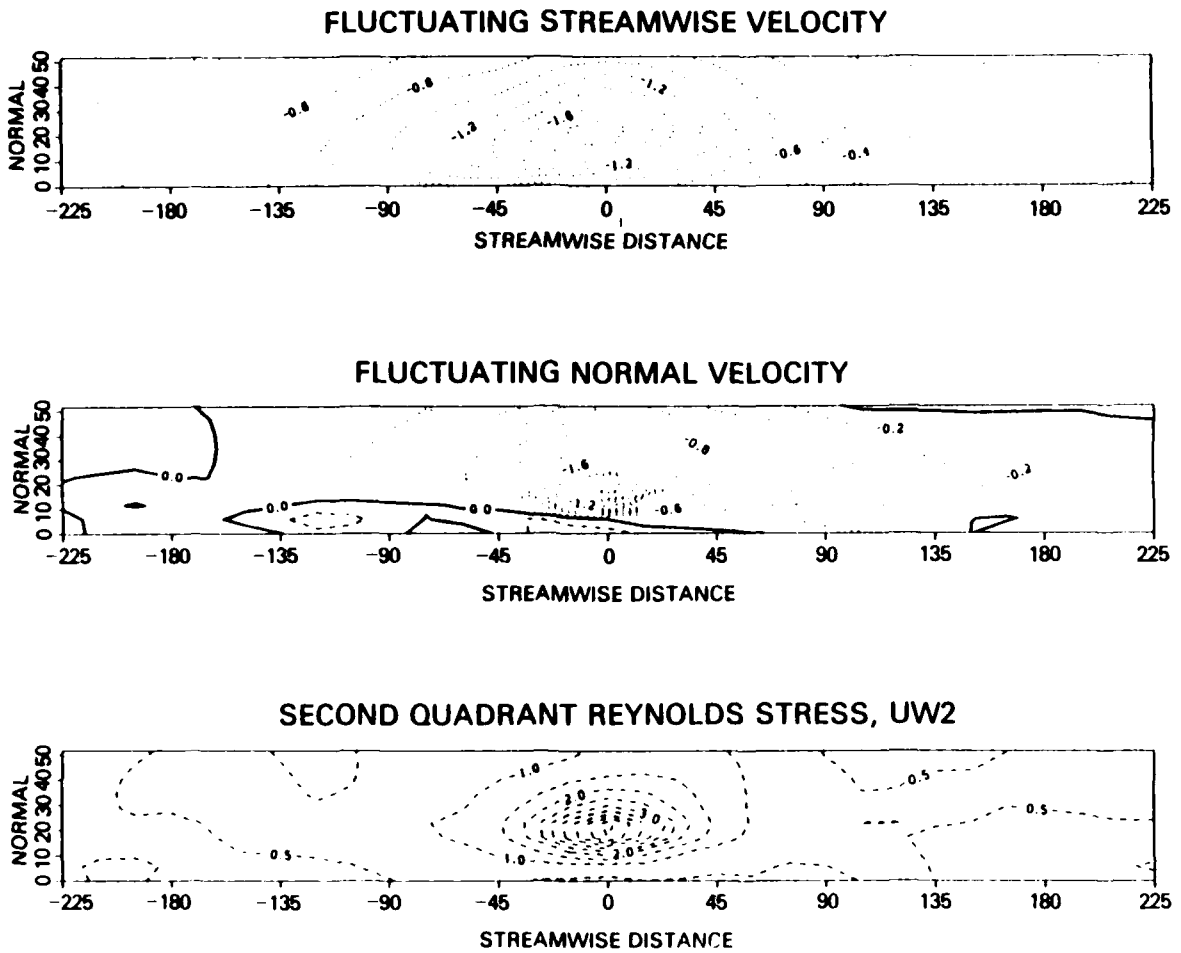

Fig. 9 — The ensemble-averaged fluctuating velocity and the second quadrant Reynolds stress, normalized using u^* for a turbulent burst detected using the second quadrant Reynolds stress detection scheme. The flow was sampled at $x_2^* = 16.5$ and K = 4, the threshold constant. Note that, due to the coordinate system used, a negative normal velocity implies the ejection of fluid away from the wall.

Appendix

For completeness we include here more detailed plots of the mean streamwise velocity and the root mean square streamwise velocity.

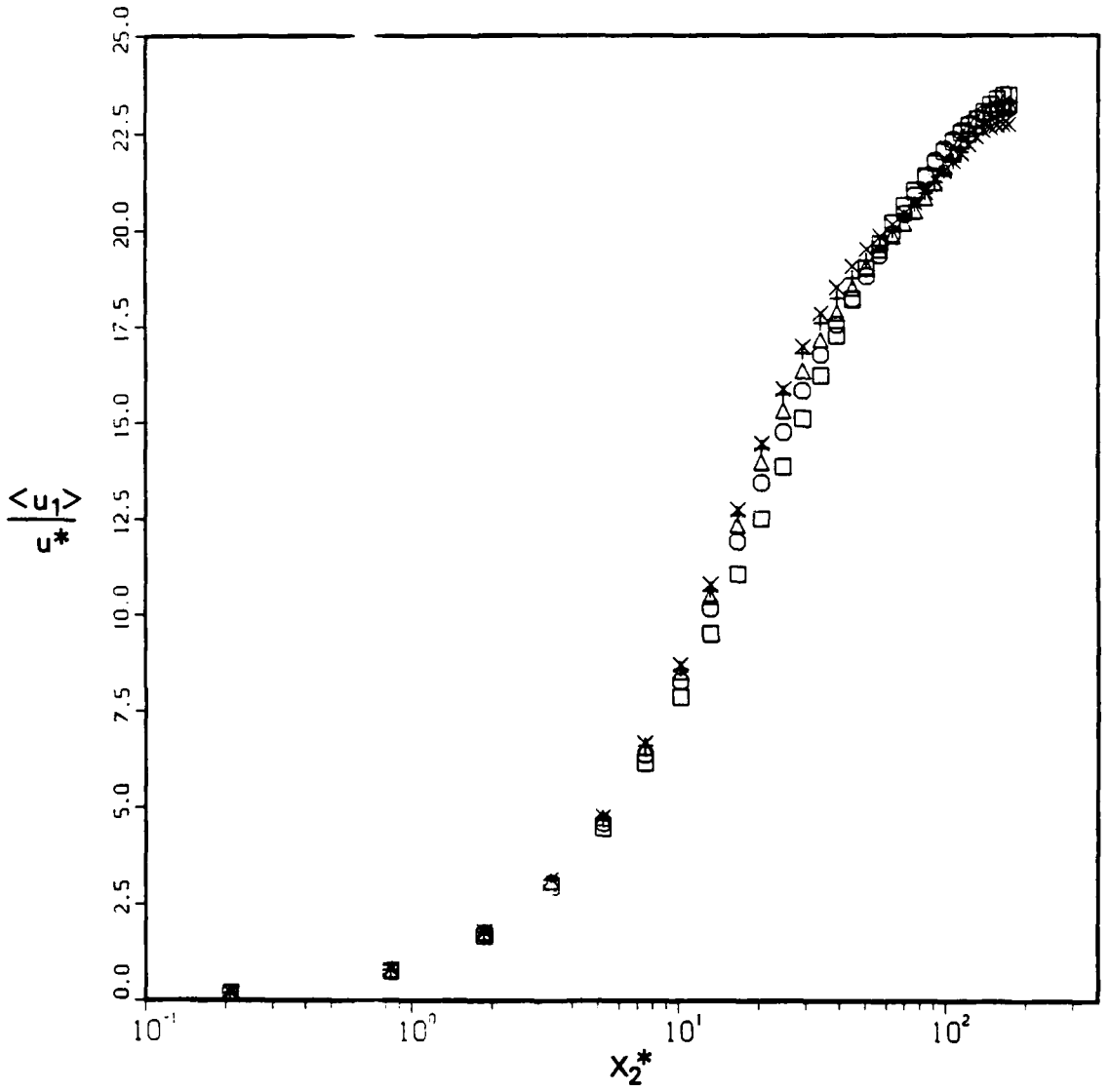

Fig. A1 — Mean streamwise velocity versus distance from the wall.

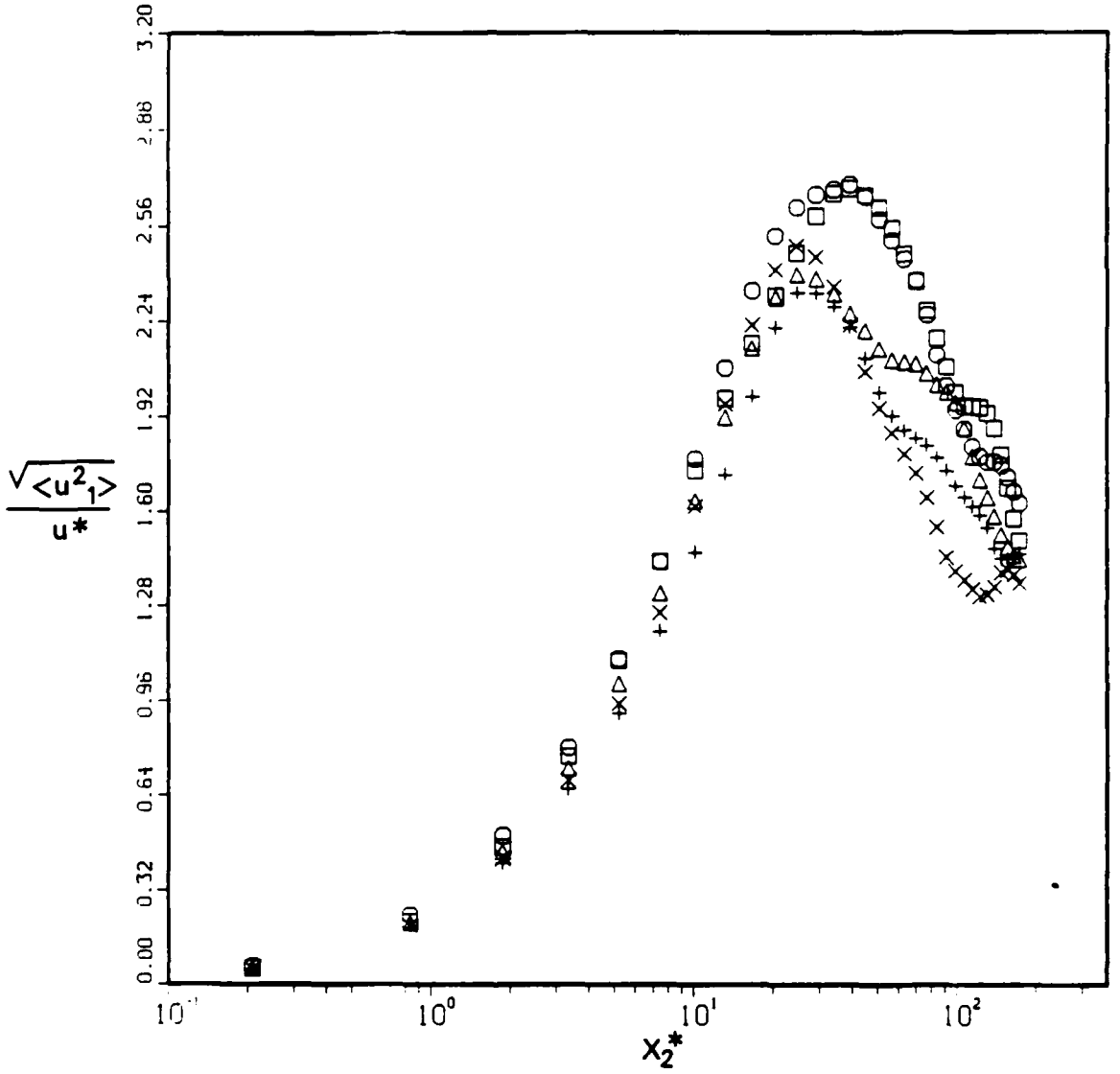

Fig. A2 — Root mean square streamwise velocity versus distance from the wall.

END

DATE

FILMED

DEC.

1987